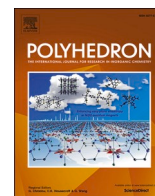




Since January 2020 Elsevier has created a COVID-19 resource centre with free information in English and Mandarin on the novel coronavirus COVID-19. The COVID-19 resource centre is hosted on Elsevier Connect, the company's public news and information website.

Elsevier hereby grants permission to make all its COVID-19-related research that is available on the COVID-19 resource centre - including this research content - immediately available in PubMed Central and other publicly funded repositories, such as the WHO COVID database with rights for unrestricted research re-use and analyses in any form or by any means with acknowledgement of the original source. These permissions are granted for free by Elsevier for as long as the COVID-19 resource centre remains active.



Synthesis and crystal structures of new mixed-ligand schiff base complexes containing *N*-donor heterocyclic co-ligands: Molecular docking and pharmacophore modeling studies on the main proteases of SARS-CoV-2 virus (COVID-19 disease)

Liana Ghasemi^a, Maryam Hasanzadeh Esfahani^a, Alireza Abbasi^b, Mahdi Behzad^{a,*}

^a Faculty of Chemistry, Semnan University, Semnan, Iran

^b School of Chemistry, College of Science, Tehran University, Tehran, Iran

ARTICLE INFO

Keywords:

COVID-19

Docking

Pharmacophore

Mixed-ligand

Unsymmetrical Schiff base

ABSTRACT

Three new mixed-ligand copper(II) complexes (**1–3**) with NN'O type unsymmetrical tridentate Schiff base ligands (**SB**) and *N*-donor heterocyclic co-ligands, with general formula [Cu(SB)(L)]ClO₄, were synthesized and characterized using single crystal x-ray diffraction (SCXRD), FT-IR and UV-Vis spectroscopy and elemental analyses. The SB ligand is the half-unit form of the condensation of 1,3-propanediamine with 5-methoxysalicylaldehyde and the co-ligands (L) are pyridine (py in (**1**)), 2,2'-bipyridine (bpy in (**2**)) and 1,10-phenanthroline (phen in (**3**)). Crystal structures of (**2**) and (**3**) were obtained by SCXRD. Molecular docking and pharmacophore studies were performed to study the interactions between the synthesized complexes and SARS-CoV-2 virus main proteases (PDB IDs: 6LU7, 6WQF and 6W9C). Results revealed that complex (**3**) with phen co-ligand showed better docking scores with the three receptors, i.e. 6LU7 (−8.05 kcal.mol^{−1}), 6W9C (−7.70 kcal.mol^{−1}) and 6WQF (−7.75 kcal.mol^{−1}). The order of the binding best energies for (**3**) was also as follows: 6LU7 > 6WQF > 6W9C. All of the studied complexes showed considerable performance, comparable to the standard drug, Favipiravir.

1. Introduction

Schiff bases (SBs) have a specific role as chelating ligands and SB complexes with transition metal ions have been studied in different fields such as catalyst, photocatalyst, corrosion inhibition, magnetism and biochemistry due to having various physical and chemical properties [1–4]. From the pharmacological point of view, they have shown antibacterial, antifungal, anti-inflammatory, antioxidant, anti-proliferative, etc. activity and numerous studies have been performed to develop efficient medicines with SB backbone [5–8].

According to the World Health Organization (WHO), the novel coronavirus COVID-19 was informed pandemic at 2019 and over 270 million people were infected by the end of 2021. Various studies have been directed to find efficient medicines for this disease [9]. Molecular docking is an efficient tool that is used to study the interactions between two or more molecular structures, e.g. drugs and proteins or enzymes [10]. This method is aimed to study the interactions of small molecules

in the binding pockets of the target proteins to identify the correct poses of the ligands in such binding pockets [11].

Considering the above mentioned, in this study, we report the synthesis and characterization of new Cu(II) mixed-ligand Schiff base complexes by various spectroscopic techniques including SCXRD. The SB complex (**1**) with NN'O type unsymmetrical main ligand and pyridine co-ligand was synthesized following a template method using 1,3-propanediamine, 5-methoxysalicylaldehyde, pyridine, and copper(II) perchlorate hexahydrate. The other target complexes were synthesized from (**1**) with ligand exchange of the monodentate pyridine by bidentate ligands. The molecular docking was employed to study the interactions between these complexes and the main proteases (MPros) of the SARS-CoV-2 virus (PDB IDs: 6LU7, 6WQF, and 6W9C) [12,13]. The studied MPros are shown to be the key for SARS-CoV-2 virus replication which makes it the potent target for inhibitor drugs [14–16]. Our results show that the synthesized complexes showed great interaction with the studied three main proteases of COVID-19. These data could be used for

* Corresponding author.

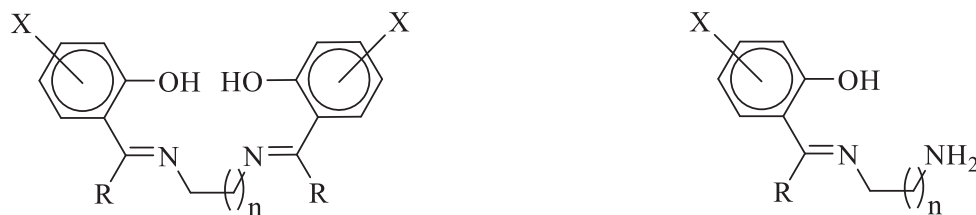
E-mail address: mbehzad@semnan.ac.ir (M. Behzad).

<https://doi.org/10.1016/j.poly.2022.115825>

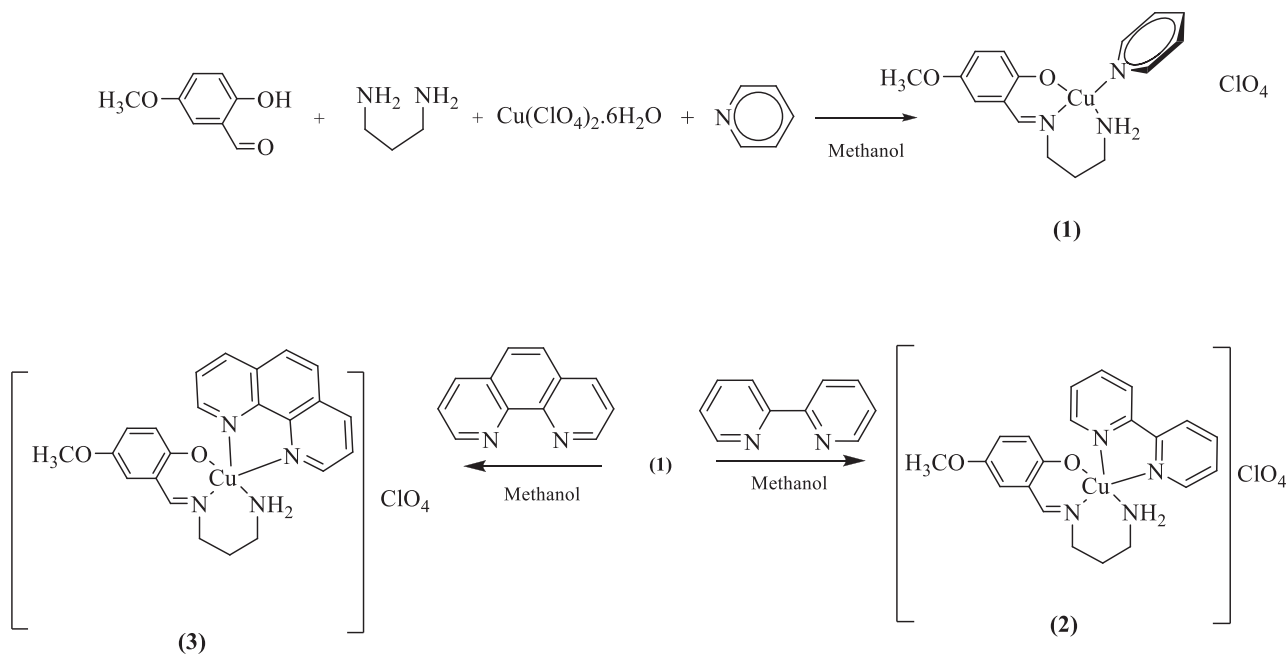
Received 21 January 2022; Accepted 1 April 2022

Available online 4 April 2022

0277-5387/© 2022 Elsevier Ltd. All rights reserved.



Scheme 1. Doubly-condensed symmetrical (left) and mono-condensed unsymmetrical (half-unit, right) Schiff base ligands from aliphatic diamines.



Scheme 2. Synthesis route for the preparation of the complexes.

rational drug design against this disease.

2. Experimental

2.1. Materials and instruments

The starting materials and solvents were purchased from commercial vendors and were consumed without re-purification. Fourier transform infrared spectra were obtained using KBr pellets by a Shimadzu 8400S device in the area from 400 to 4000 cm^{-1} . The ultraviolet–visible absorption spectra were obtained on a Shimadzu UV-1650 PC apparatus using a quartz cuvette and methanol as the solvent and reference. The elemental analyses were done on an Eager 300 for EA1112 analyzer. The X-ray diffraction measurements were carried out on a MAR345 dtb diffractometer equipped with an image plate detector using $\text{Mo-K}\alpha$ X-ray radiation. The structures were solved by direct methods using SHELXS-97 and refined using full-matrix least-squares method on F2, SHELXL [17,18]. All non-hydrogen atoms were refined anisotropically.

2.2. Molecular docking studies

Molecular docking simulations were performed using the software AutoDock 4.2. The crystallographic data for complexes (2) and (3) were exported as a CIF file and converted to PDB format using Mercury software. The complex (1) was optimized via standard 6-311G** basis sets which were used for C, H, N, and O atoms while the LANL2DZ basis set along with the effective core potential (ECP) functions were

employed for Cu. The crystal structures of SARS-CoV-2 primary proteases (PDB IDs: 6LU7, 6W9C, and 6WQF) were downloaded from Protein Data Bank (<https://www.rcsb.org>) and the standard drug was downloaded from PubChem. By eliminating all water molecules, assigning Gasteiger partial charges, and adding polar hydrogen, the 6LU7/6W9C/6WQF proteins structures were created. A grid box with $116 \times 100 \times 126 \text{ \AA}$ points and a grid-point spacing of 0.636 was used to create docking simulations for 6LU7. For 6W9C and 6WQF the grid box with $126 \times 126 \times 126 \text{ \AA}$ points and the same spacing was used. A Lamarckian genetic algorithm method was also employed in this investigation. The number of assessments and genetic algorithm runs were limited to 200. We looked at the constructions and chose the ones with the lowest energy among those that were similar. The interactions of 6LU7/6W9C/6WQF with the complexes, as well as their binding modalities, were then investigated using the AutoDock program, UCSF Chimera 1.5.1 software, Accelrys Discovery Studio 3.0, and DS Visualizer, LigPlus [12,19–21].

2.3. Pharmacophore profile

Pharmit link (<https://pharmit.csb.edu>) was used to search for pharmacophore modeling. This study aims to investigate interaction features between Cu(II) complexes to coronavirus variation structures as a receptor. The number of H-bond acceptor (H-acc.), H-bond donor (H-don.), Hydrophobic (Hyd.) were also reported [22].

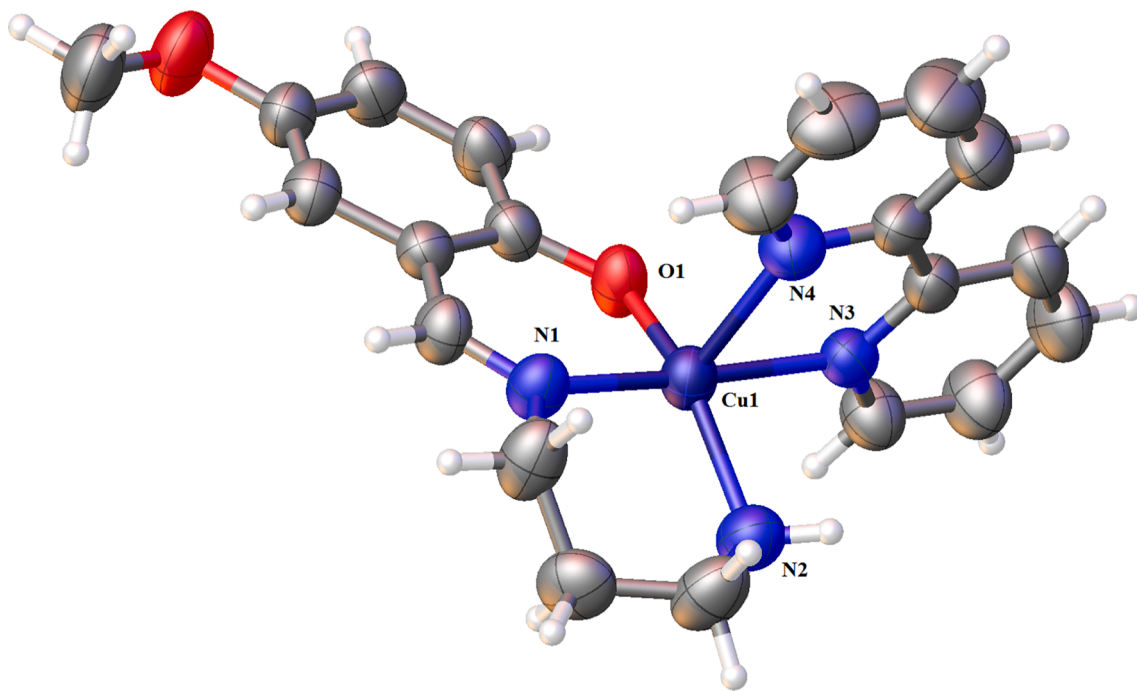


Fig. 1. Molecular structure of (2) with atom numbering scheme. Thermal ellipsoids are drawn at 50% probability level. Hydrogen atoms are drawn as small spheres with arbitrary radii. The disordered perchlorate anion is emitted for clarity.

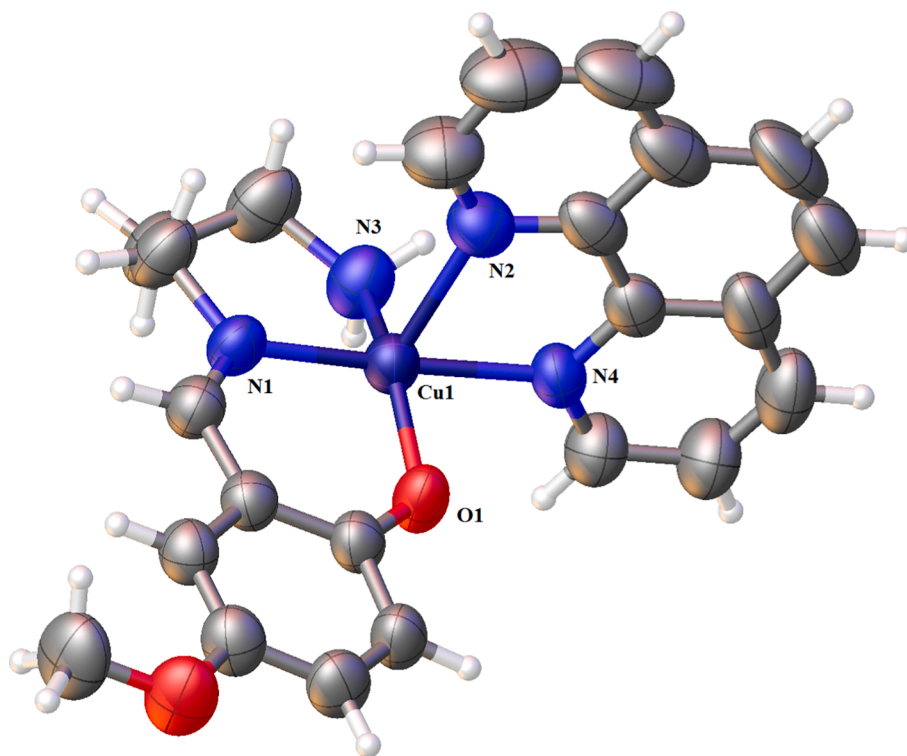


Fig. 2. Molecular structure of (3) with atom numbering scheme. Thermal ellipsoids are drawn at 50% probability level. Hydrogen atoms are drawn as small spheres with arbitrary radii. The perchlorate anion is emitted for clarity.

2.4. Synthesis of the complexes

2.4.1. Synthesis of $[Cu(L)(py)]ClO_4$ (1)

In a typical experiment, 0.76 g of 2-hydroxy-5-methoxybenzaldehyde (5.00 mmol) was dissolved in 30 mL of methanol in a round-bottom flask. While this solution was being continuously stirred at

room temperature, 5 mL of an aqueous solution of $Cu(ClO_4)_2 \cdot 6H_2O$ (5.00 mmol, 1.85 g) was slowly added, followed by the addition of 0.80 g (10.00 mmol) of pyridine. The reaction mixture was stirred for 1 h. 0.37 g of 1,3-propanediamine (5.00 mmol), dissolved in 5 mL of methanol, was then added dropwise to the reaction mixture. This reaction mixture was further stirred for 3 h without heating. The green

Table 1

A summary of the crystallographic data.

Crystal data	(2)	(3)
Empirical formula	C ₂₁ H ₂₃ CuN ₄ O ₂ ClO ₄	C ₂₃ H ₂₃ CuN ₄ O ₂ ClO ₄
Formula weight	526.42	550.44
Crystal system	Monoclinic,	Monoclinic,
Space group	P2 ₁ /c	P2 ₁ /c
Unit Cell dimensions (Å,°)		
a, b, c (Å)	8.7669 (18), 22.046 (4), 12.186 (2)	8.6308 (17), 23.835 (5), 11.987 (2)
β (°)	97.50 (3)	98.37 (3)
Volume (Å ³)	2335.1 (8)	2439.6 (8)
Z	4	4
Radiation type	Mo K _α	Mo K _α
Absorption coefficient (mm ⁻¹)	1.09	1.05
No. of measured, independent and observed [I > 2σ(I)] reflections	14563, 4074, 3442	14926, 4157, 3877
T _{min} , T _{max}	0.865, 1.182	0.882, 1.164
R _{int}	0.082	0.059
R[F ₂ > 2σ(F ₂)], wR(F ₂), S	0.067, 0.172, 1.11	0.066, 0.181, 1.11
No. of parameters	308	317
Δρ _{max} , Δρ _{min} (e Å ⁻³)	0.62, -0.30	0.73, -0.44

Table 2

Selected bond lengths and angles around the central metal ion in (2) and (3).

Bond lengths (Å)			Bond angles (°)		
Bond	(2)	(3)	Angle	(2)	(3)
Cu1-O1	1.929 (3)	1.920 (3)	O1-Cu-N1	93.41 (15)	93.56 (14)
Cu1-N1	1.978 (4)	1.978 (4)	O1-Cu-N2	149.78 (18)	103.24 (15)
Cu1-N2	2.023 (4)	2.294 (4)	O1-Cu-N3	86.71 (14)	151.97 (18)
Cu1-N3	2.057 (4)	2.023 (4)	O1-Cu-N4	105.00 (16)	86.09 (13)
Cu1-N4	2.266 (4)	2.067 (4)	N1-Cu1-N2	94.66 (18)	98.79 (16)
			N1-Cu1-N3	175.88 (17)	95.50 (16)
			N1-Cu1-N4	99.90 (17)	175.22 (16)
			N3-Cu1-N2	87.26 (17)	101.50 (17)
			N3-Cu1-N4	76.11 (15)	86.97 (15)
			N2-Cu1-N4	102.20 (17)	76.68(15)

Table 3

Hydrogen bond geometry (Å, °).

D-H...A	D-H	H...A	D...A	D-H...A
(2)				
N(2)-H(2A)...O(5)	0.89	2.45	3.326	169
N(2)-H(2A)...O(7)	0.89	2.39	3.154	143
(3)				
N(3)-H(3A)...O(6)	0.89	2.40	3.278	171
N(3)-H(3B)...O(4)	0.89	2.43	3.309	172

precipitate was collected by filtration and washed with diethyl ether and air-dried. The obtained powder was recrystallized from methanol to give needle-shaped polycrystals of the target complex. The yield was 1.81 g (81.2 %). Selected IR (cm⁻¹) 3440, 3304, 3256, 2943, 1610, 1486, and 1100. UV-Vis. 10⁻⁵ M solution in methanol [λ_{max} nm (ε, M⁻¹cm⁻¹): 224 (32000), 252 (26000), 276 (13000), 662 (90)]. Anal. Calcd. (Found) for C₁₆H₂₀ClCuN₃O₆: C, 42.77 (42.62); H, 4.49 (4.60); N, 9.35 (9.17).

2.4.2. Synthesis of [Cu(L)(bpy)]ClO₄ (2)

1 mmol, 0.44 g of (1) was suspended in 10 mL of methanol and then, 5 mL of methanolic solution of 2,2'-bipyridine (2 mmol, 0.31 g) was slowly added to the reaction mixture. The reaction mixture was stirred for 3 h. Green sediment was collected by filtration and washed with 20 mL diethyl ether and air dried. The yield was 0.42 g (76.6 %). Pure crystals were obtained by slow evaporation of a methanolic solution.

Selected IR (cm⁻¹): 3321, 3271, 2935, 1631, 1595, 1539, 1473, 1461, 1269 and 1095. UV-Vis. 10⁻⁵ M solution in methanol [λ_{max} nm, (ε, M⁻¹cm⁻¹): 231 (61000), 272 (42000), 405 (5800), and 653 (120)]. Anal. Calcd. (Found) for C₂₁H₂₂ClCuN₄O₆: C, 47.87 (47.71), H, 4.36 (4.46), N, 10.63 (10.50).

2.4.3. Synthesis of [Cu(L')(phen)]ClO₄ (3)

This complex was prepared following a similar procedure as described for (2) except 0.36 g, 2.00 mmol of 1,10-phenanthroline was used instead of 2,2'-bipyridine. Pure crystals were obtained by slow evaporation of a methanolic solution. The yield was 0.49 g (93.5 %) Selected IR (cm⁻¹): 3323, 3276, 2937, 1629, 1541, 1515, 1475, 1432, 1218, 1097. UV-Vis 10⁻⁵ M solution in methanol [λ_{max} nm, (ε, M⁻¹cm⁻¹): 234 (41000), 278 (28000), 402 (6400) and 664 (110)]. Anal. Calcd. (found) for C₂₃H₂₃ClCuN₄O₆: C, 50.13 (50.20); H, 4.18 (4.35); N, 10.17 (10.35).

3. Results and discussion

3.1. Synthesis

Salen-type tetradentate SBs are the most-widely studied SB ligands and are categorized as symmetrical and unsymmetrical SBs [7]. Such symmetrical ligands contain diamines that have a plane of symmetry (such as ethylenediamine and 1,3-propanediamine) which are doubly condensed with the same aldehyde or ketone (Scheme 1). These N₂O₂ type symmetrical SBs could be more easily synthesized while the synthesis of their corresponding mono-condensed NN'O forms (the so-called half-units, Scheme 1) is extremely difficult. Our attempts to synthesize and isolate such half-units have usually failed. On the other hand, we have adopted and developed a template method which gives the transition metal ion complexes with tridentate NN'O type SB ligands accompanied by a monodentate N-donor heterocyclic co-ligand (here, py) [8]. The monodentate co-ligand could be easily replaced by other co-ligands such as 2,2'-bipyridine, etc. to give a variety of new complexes. Scheme 2.

The obtained complexes were very soluble in polar aprotic solvents such as DMF, DMSO, CH₃CN and were also soluble in other polar solvents such as methanol, ethanol and dichloromethane. The complexes were stable below about 200 °C but decomposed above it. This is usual for the perchlorate salts which decompose, sometimes explosively at elevated temperatures.

3.2. X-ray crystallography

Single crystals suitable for x-ray crystallography were grown by slow evaporation of the methanolic solution of the complexes over a week or two. Fig. 1 shows the molecular structure of (2) with atom numbering Scheme. Molecular structure of (3) is also shown in Fig. 2. The crystallographic data and the refinement parameters are collected in Table 1. Table 2 contains the selected bond lengths and angles around the central metal ion.

3.2.1. Description of the crystal structure of (2)

The molecular structure of (2) is consisted of one complex cation together with a disordered perchlorate anion in the asymmetric unit. Two perchlorate oxygen atoms are disordered in three positions with refined occupancy factors of O3/0.65, O6/0.75 and O7/0.6. As could be seen from Fig. 1, the central Cu(II) metal ion is penta-coordinated and the geometry around the central metal ion is distorted square-based pyramid (SBP). The four basal positions are formed by the three donating groups from the unsymmetrical Schiff base ligand along with one nitrogen atom from the bpy ligand, locating in quasiplanar fashion with a rms deviation of 0.2817 Å for the fitted 4 atoms. The Schiff base ligand is coordinated to the central metal ion via the N atom of the uncondensed NH₂ group, N atom from the C=N, and the O atom from

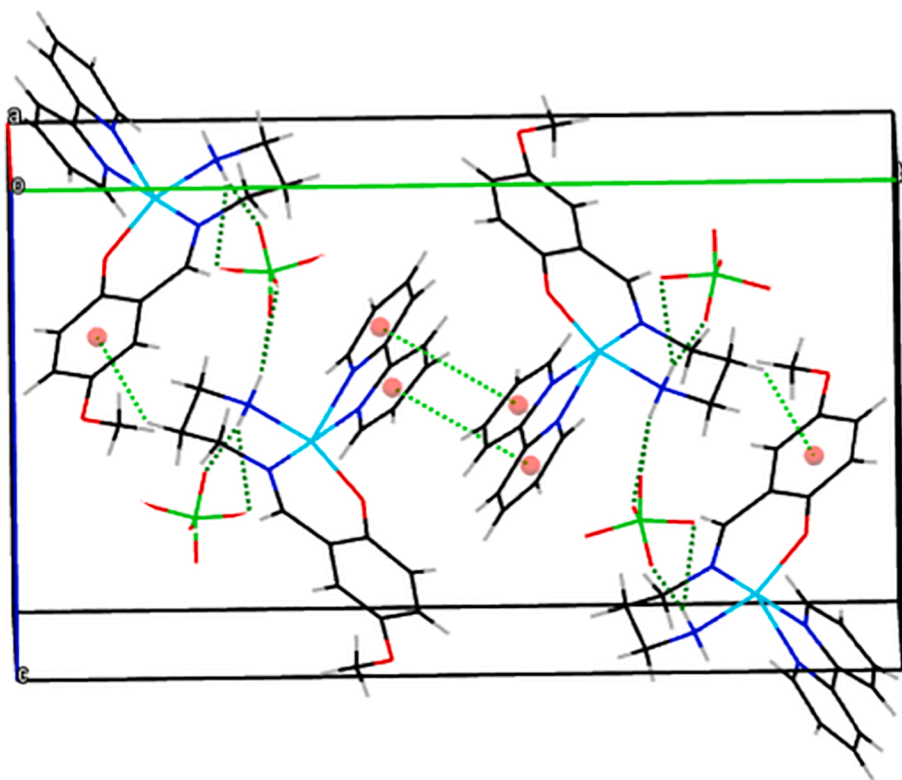


Fig. 3. Crystal packing for (2) along b axis.

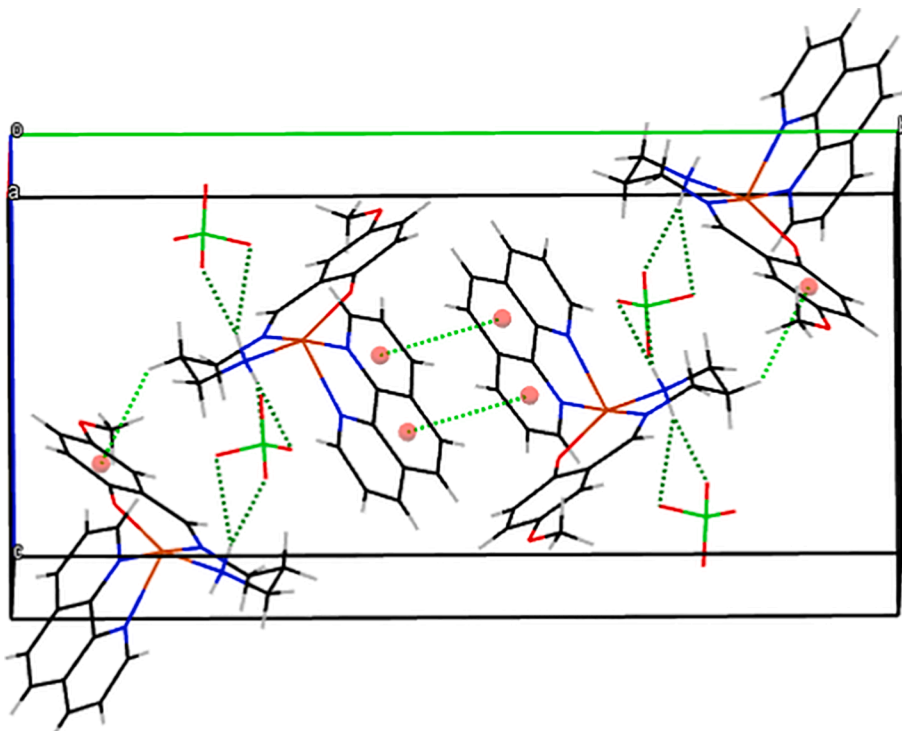


Fig. 4. Crystal packing for (3) along b axis.

the deprotonated phenolic group. This ligand is mono-anionic, and since the other ligand i.e. bpy is neutral, the complex has a (+1) charge which is compensated by the negatively charged perchlorate anion. The apical position of the SBP is also occupied by the other N atom from the bpy ligand. The geometry index (τ) which was calculated from $\tau = (\beta - \alpha) / 60$

is equal to 0.435 [21]. This value is zero for the ideal SBP while it is equal to 1 for ideal trigonal bipyramidal (TBP) geometry. In this equation, β and α are the two greatest bond angles around the central metal ions, respectively. The value of (τ) is almost between the two limiting values but it is slightly closer to that of SBP and hence, the geometry

Table 46LU7 docking results of the complexes (1), (2), and (3) and Favipiravir (kcal.mol⁻¹).

	SB	(1)	(2)	(3)	Favipiravir
Estimated free energy of binding ^a	-5.48	-6.95	-7.31	-8.05	-3.81
Final intermolecular energy	-7.56	-7.54	-7.61	-8.34	-4.11
vdW + H-bond + desolve Energy	-5.70	-7.08	-7.32	-7.92	-4.05
Electrostatic energy	-1.86	-0.46	-0.29	-0.42	-0.06
Final total internal energy	-0.19	-0.36	-0.04	-0.04	-0.08
Torsional free energy	2.09	0.60	0.30	0.30	0.30
Unbound system's energy	-0.19	-0.36	-0.04	-0.04	-0.08

$$^a \Delta G_{\text{binding}} = \Delta G_{\text{vdW}} + \text{hb} + \text{desolve} + \Delta G_{\text{elec}} + \Delta G_{\text{total}} + \Delta G_{\text{tor}} - \Delta G_{\text{unb.}}$$

could be described as distorted SBP [22]. The obtained bond lengths, bond angles, and the (τ) value is in the same range of previously reported similar complexes [23,24]. The weak hydrogen bonds N—H...O, Table 3, together with the CH- π and π - π stacking interactions stabilize the entire 3D Network structure (Fig. 3).

3.2.2. Description of the crystal structure of (3)

Crystal structure of (3) is very much similar to (2). It consists of one complex together with one perchlorate ion in the asymmetric unit. As could be seen from Fig. 2, the Schiff base ligand in this complex is also deprotonated from the phenolic OH and is monoanionic. The value of τ for this complex is 0.388 and again, the geometry around the central metal ion could be considered as distorted SBP. The four basal planes are occupied by the three NN'O donating groups of the Schiff base ligand and one N atom of the 1,10-phenanthroline co-ligand, forming a quasiplanar mode with a rms deviation of 0.2684 Å. The apical position is also occupied by the other N atom of phen. The obtained bond lengths, bond angles, and the (τ) value is in the same range of previously reported similar complexes. The weak hydrogen bonds N—H...O, Table 3, as well as the CH- π and π - π stacking interactions are responsible to stabilize the 3D crystal structure (Fig. 4).

3.3. Description of the IR and UV-Vis spectra

The IR and UV-Vis spectroscopic data could be easily explained based on the obtained crystallographic data. In the FTIR spectra of the three complexes (Supplemental Fig. S.1-3), three characteristic peaks were expected. The first important feature was the observation of an intense signal at around 1630 cm⁻¹. This signal was indicative of the formation of the imine bond and hence, the presence of the SB ligand. The other medium intensity and doubly-split sharp signals at around 3400–3200 cm⁻¹ confirm the presence of the NH₂ group which is indicative of the formation of half-unit. The last important signals which were observed at around 1100 cm⁻¹ indicated the presence of perchlorate anion. These data are similar to the previously reported complexes with the same backbone [25].

In the electronic spectra of the complexes (Supplemental Fig. S.4-6), four signals were observed. The two high intensity and energy signals which were observed below 300 nm where assigned to the $\pi \rightarrow \pi^*$ transitions. The medium intensity signal at around 400 nm could be assigned to the MLCT and the very low intensity signals above 600 nm, which were only observed at higher concentrations could also be easily assigned to the d \rightarrow d transitions [26].

3.4. Molecular docking with SARS-CoV-2 virus as receptor (PDB ID:6LU7) protein

The coronavirus illness (COVID-19) epidemic has caused severe damages all around the world. A lot of researches have been conducted to find new and effective drugs for this disease. Molecular docking is a great tool to study the drug/receptor interactions and is used to discover

factors affecting the effectiveness of the drugs towards a special disease [10,12]. Metal-based drugs have also been examined both theoretically and clinically to cure some diseases such as cancer, etc. Both ligands and the central metal ion are important. Schiff bases are considered to be very important classes of ligands, in this regard, and various Schiff base complexes have been examined as potential metallodrugs. In this study, we examined the interaction of three new Schiff base complexes with 6LU7/6W9C/6WQF proteins of SARS-CoV-2. The values of docking energies were -5.48, -6.95, -7.31, -8.05, and -3.81 kcal.mol⁻¹ for (SB), (1), (2), (3), and Favipiravir, respectively (Table 4 and Fig. 5). In the ligand (SB), three H. bondings were found between the aldehyde OH, and the two H atoms of the NH₂ group, to the oxygen atoms of GLU166, PHE140 and GLU166 at 2.17, 2.11 and 1.88 Å. One C—H. bondings was found between the C of amine to the oxygen atoms of LEU141 at 3.28 Å. One π - σ Hyd. was found between the C of OCH₃ to HIS41 at 3.76 Å. One π -Alkyl Hyd. was also found between the aldehyde ring to MET165 at 5.38 Å. In complex (1), three H. bondings were found between the hydrogen atoms of the NH₂ group from SB ligand to the oxygen atoms of GLU14, MET17, and GLY120 at 2.38, 2.20, and 2.33 Å. Three C—H. bondings to VAL18, GLN19, and MET17 were found at 3.65, 3.54, and 2.84 Å. Alkyl Hyd. to ALA70 was also found at 3.95 Å. In (2), the H. bonding between the hydrogen of NH₂ group to the oxygen atom of ASN142 was found at 2.67 Å. In addition, six Alkyl Hyd. bonds were found between bpy and phenyl rings to MET49, MET165, LEU27, and CYS145 at 4.94, 4.96, 5.44, 5.47, 4.53 and 3.74 Å, respectively. Three π -Alkyl Hyd. bondings were also found between HYS41 and HYS163 to the aldehyde and bpy rings at 5.41, 4.34 and 4.85 Å. In complex (3), one H. bonding between the hydrogen atom of the NH₂ group on the complex was found to the oxygen atom of ASN142 at 2.11 Å. Three Alkyl Hyd. were also found between ph ring and aldehyde ring to CYS145 and MET165 at 3.86, 5.39 and 4.66 Å. One π -Alkyl Hyd. bond between HYS163 to (3) was found at 5.30 Å. The drug-receptor residue interactions between ligand (SB), complexes and the standard drug Favipiravir, with 6LU7, are shown in Supplemental table S.1. It could be rationalized that the main Schiff base ligand has greater effect on the interactions, since the interactions involving this ligand appear at lower distances and hence, are stronger. It could also be seen that the H. bonds and Alkyl Hyd. bonds result in better binding of the complexes to the studied proteins. Complex (3) has more negative binding energies and the energies are spontaneous and negative. Besides, all the synthesized complexes have more negative binding energies than Favipiravir.

The obtained docking results for the complex (3) has shown the best binding energy with 6LU7 (-8.05 kcal.mol⁻¹). Hydrogen bond interactions has made the complex stable and the inclusion of oxygen of methoxy group, phen ring, and aldehyde ring in the structure has resulted in good inhibitory activities, which is attributed to the establishment of good bonding interactions with 6LU7.

3.5. Molecular docking with SARS-CoV-2 virus as receptor (PDB ID: 6W9C) protein

Another structure of coronavirus is papain-like protease of SARS CoV-2 (6W9C) [19]. We examined, in this study, the effect of the ligand (SB) and complexes (1), (2), and (3), as well as Favipiravir with 6W9C. The values of docking energies for (SB), (1), (2), (3), and Favipiravir were -5.15, -6.32, -7.0, -7.70, and -4.86 kcal.mol⁻¹, respectively (Table 5 and Fig. 6). When relative binding energies ($\Delta G_{\text{binding}}$) were compared, complex (3) performed better than ligand (SB), complexes (1), (2) and the standard drug Favipiravir. Table S.2 shows the drug-receptor residue interactions between the complexes and Favipiravir with 6W9C. In ligand (SB), three H. bonding between O of OCH₃, OH of Aldehyde and H of NH₂ to PHE79, THR74 and PRO59 were found at 2.97, 1.90 and 1.93 Å. One C—H. bond was found between C of OCH₃ to PRO77 at 2.79 Å. Two Alkyl Hyd. between C of OCH₃ to LEU58 and LEU80 at 4.69 and 3.50 Å. Three π -Alkyl Hyd. between ring of Aldehyde to PRO59, ALA68 and LEU80 were found at 4.75, 4.51 and 5.08 Å. In

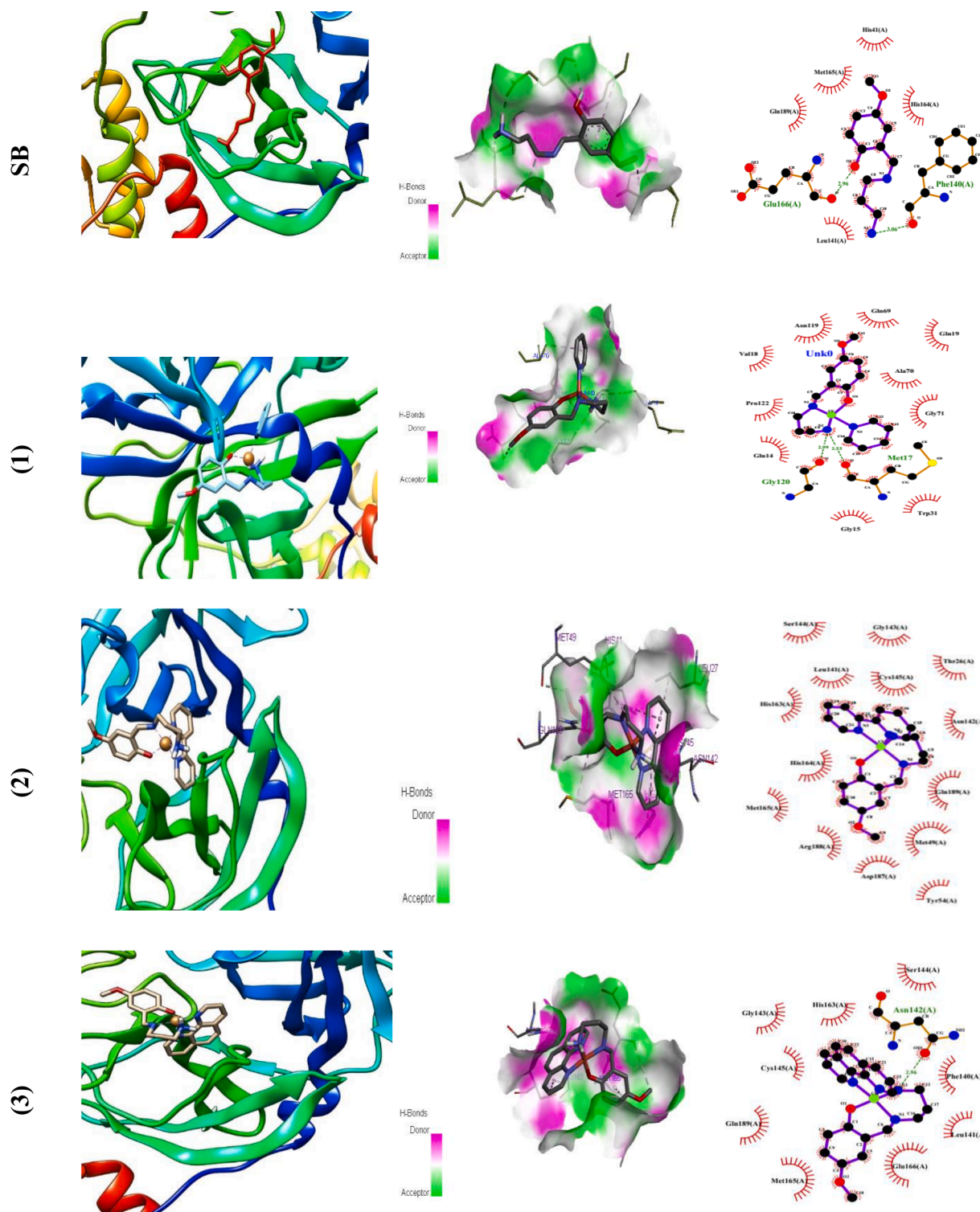


Fig. 5. The molecular docking results of (SB), (1), (2), (3) and Favipiravir with 6LU7. (a) Molecular docking (b) H. bond Receptor-side surface interactions and (c) 2D-diagram representations.

complex (1), three H. bonding between NH_2 of ligand to ASN156, GLU161 was found at 2.26, 2.81 and 2.68 Å. Alkyl Hyd. and π - Alkyl Hyd. to LYS92 and TRP93 were found at 4.79 and 5.45 Å. In complex (2), H. bonding between O of Aldehyde to ASN109 was found at 2.15 Å. Two alkyls Hyd. between the ring of bpy and aldehyde to LEU162 were found at 4.83 and 5.29 Å. In complex (3), Two H. bonding between O1 and H3B of NH_2 to ASN109 and GLY160 were found at 2.95, and 1.99 Å.

Four alkyl hyd. bonds were also found between LEU162 and ph ring of the aldehyde moiety at 5.34, 4.87, 5.05 and 3.50 Å. In Favipiravir, three H. bonds between LEU80, THR74, and PRO77 were found at 1.81, 2.18, and 2.26 Å. One C—H. bond between ligand and THR75 was found at 3.36 Å. The π - σ Hyd. between ph ring of the ligand to PRO59 was found at 3.99 Å. Two π - Alkyl Hyd. between ph ring of the ligand were found 4.81 and 4.93 Å.

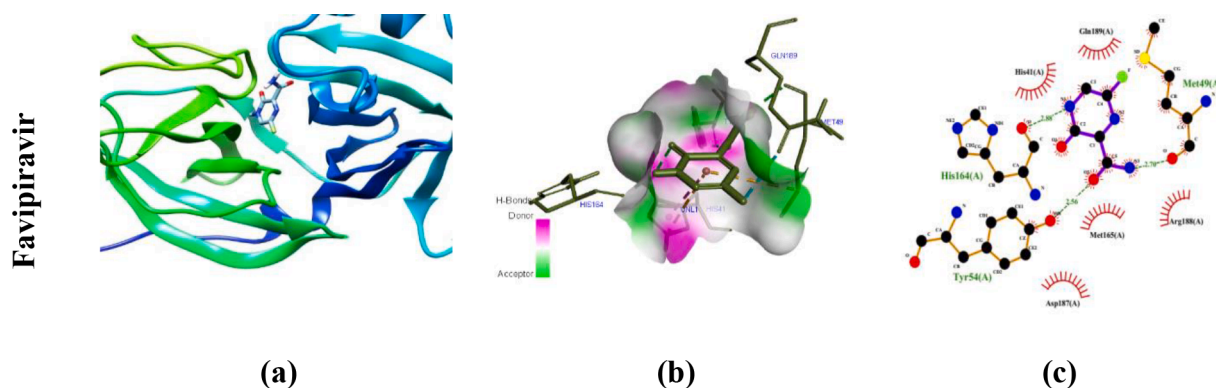


Fig. 5. (continued).

Table 5

Docking results of the complexes (1), (2), and (3) and Favipiravir to 6W9C (kcal. mol⁻¹).

	SB	(1)	(2)	(3)	Favipiravir
Estimated free energy of binding ^a	-5.15	-6.32	-7.0	-7.70	-4.86
Final intermolecular energy	-7.24	-6.92	-7.30	-7.99	-5.16
vdW + H-bond + desolve Energy	-7.36	-5.99	-7.29	-8.00	-4.99
Electrostatic energy	0.12	-0.93	0.0	0.01	-0.16
Final total internal energy	-0.89	-0.36	-0.03	-0.04	-0.35
Torsional free energy	2.09	0.6	0.3	0.3	0.3
Unbound system's energy	-0.89	-0.36	-0.03	-0.04	-0.35

$$^a \Delta G_{\text{binding}} = \Delta G_{\text{vdW}} + \text{hb} + \text{desolve} + \Delta G_{\text{elec}} + \Delta G_{\text{total}} + \Delta G_{\text{tor}} - \Delta G_{\text{unb}}$$

The docking data with 6W9C revealed that complex (3) has the best binding energy (-7.70 kcal.mol⁻¹). H. bonding and Alkyl Hyd. interactions make the complex stable and the presence of oxygen in the methoxy group, the phen ring, and the aldehyde ring in the structures of the compounds has resulted in good inhibitory activities, which can be linked to the formation of good bonding interactions with 6W9C. In the Table 5, all the new complexes have better binding energy than the Favipiravir drug.

3.6. Molecular docking with SARS-CoV-2 virus as receptor (PDB ID: 6WQF) protein

The other SARS CoV-2 protease structure that we studied, in this paper, was the 6WQF protein [12]. The ligand (SB) and complexes (1), (2) and (3) were also compared to the standard Favipiravir drug. The values of docking energies for (SB), (1), (2), (3) and Favipiravir were -5.97, -7.66, -7.46, -7.75, and -4.19 kcal.mol⁻¹, respectively (Table 6 and Fig. 7). Like 6WC9 and 6LU7, when relative binding energies ($\Delta G_{\text{binding}}$) were compared, complex (3) performed better than (SB), complexed (1), (2), and the standard drug Favipiravir. Table S.3 shows the drug-receptor residue interactions between (SB), (1), (2), (3), and Favipiravir with 6WQF. In ligand (SB), four H. bond were found between O of OCH₃, OH of Aldehyde, and H of NH₂ (two) to GLN110, ASP295, ILE152 and ASP153 at 2.02, 2.00, 2.20 and 2.07 Å. One π -Alkyl Hyd. between C of OCH₃ to PHE294 was found at 4.65 Å. In complex (1), three H. bondings between H of NH₂ from the unsymmetrical Schiff base ligand, to GLU14, MET17, and GLY120 were found at 2.20, 2.21, and 2.28 Å. Four C—H. bonds to VAL18, GLN19, GLY71, and MET17 were found at 3.46, 3.10, 3.71 and 2.73 Å. Alkyl hyd. between the py ring to ALA70 was also found 3.41 Å. In complex (2), H. bonding between H2B of NH₂ to GLU240 was found at 1.72 Å. Two C—H. bonds between 1,3-

propanediamin to GLU40 and PRO132 were found at 2.86 and 2.87 Å. Five alkyl hyd. to PRO108 (two), PRO132, ILE200 and PRO241 were found at 4.91, 4.10, 4.64, 4.91, 4.88 Å. π -Alkyl Hyd. between bpy ring to HIS246 was found at 5.28 Å. In complex (3), one H. bonding between H3B of NH₂ to ASP153 was found at 1.88 Å. Two C—H. bonds between OCH₃ of the Schiff base to THR111 and ASP295 were found at 1.88 and 2.96 Å. Four alkyl hyd. interactions between phen ring to VAL297, ARG298, VAL303, and VAL297 were found at 5.01, 4.88, 5.24 and 5.39 Å. Two π -alkyl Hyd. between phen ring and PHEN294 were found at 4.70 and 4.62 Å. In Favipiravir, two H. bonds, two H. bond intermolecular, and a C—H. bond were found at 2.33, 2.02, 2.13, 2.32 and 2.87 Å, respectively.

The optimum binding energy for complex (3) was discovered to be -7.75 kcal.mol⁻¹. H. bond, C—H. bond, and Alkyl Hyd. makes the complex stable and the presence of phen ring, oxygen in the methoxy group, and NH₂ in Schiff base ligand in the structures of the compounds have been effective in molecular docking. In Table 6, all the new compounds showed better binding energies than Favipiravir.

3.7. Pharmacophore analyses

Using Pharmit link, the maximum interactions between the new compounds and coronavirus structures (6LU7, 6WC9 and 6WQF) was obtained [27]. The initial step towards understanding how different complexes can bind to receptor, is pharmacophore. The reason why (3) had better anti-COVID-19 efficacy than (SB), (1), (2) and Favipiravir was determined by pharmacological characterization [28]. Fig. 8 depicts the pharmacophore results as well as ligand and complex-receptor interactions. As shown in Fig. 8, all of the studied chemicals interacted well with 6W9C, 6LU7, and 6WQF protein pockets. These figures are set in the best view in the Pharmit link. H. bond donor (white spheres), H. bond acceptor (orange spheres), hydrophobic rings (green spheres), and aromatic rings (purple spheres) were the four key properties of the pharmacophore developed by Pharmit link for the provided receptor data. The number of bonds counted with 6WQF, 6LU7, and 6WQC, for (SB), (1), (2) and (3) is shown in Table 7.

In Table 7, the functional groups for (SB) interacting to 6LU7 are OH of Aldehyde (HBD) and H of NH₂ ligand (HBD) which were able to make H. bond interactions; OH of aldehyde (HBA) and O of OCH₃ (HBA), and C of OCH₃ (HYD) which were able to make π - σ Hyd. interactions. Functional groups for (SB) to 6W9C were H of NH₂ (HBD) and OH of Aldehyde (HBD) which were able to make H. bond interactions; O of OCH₃ group and O of aldehyde (HBA) which were able to make H. bond interactions; Ring of Aldehyde (HYD) which was able to make π -Alkyl Hyd. interactions, C of ligand (HYD) and C of OCH₃ (HYD) which were able to make Alkyl Hyd. interactions. Functional groups for (SB) to

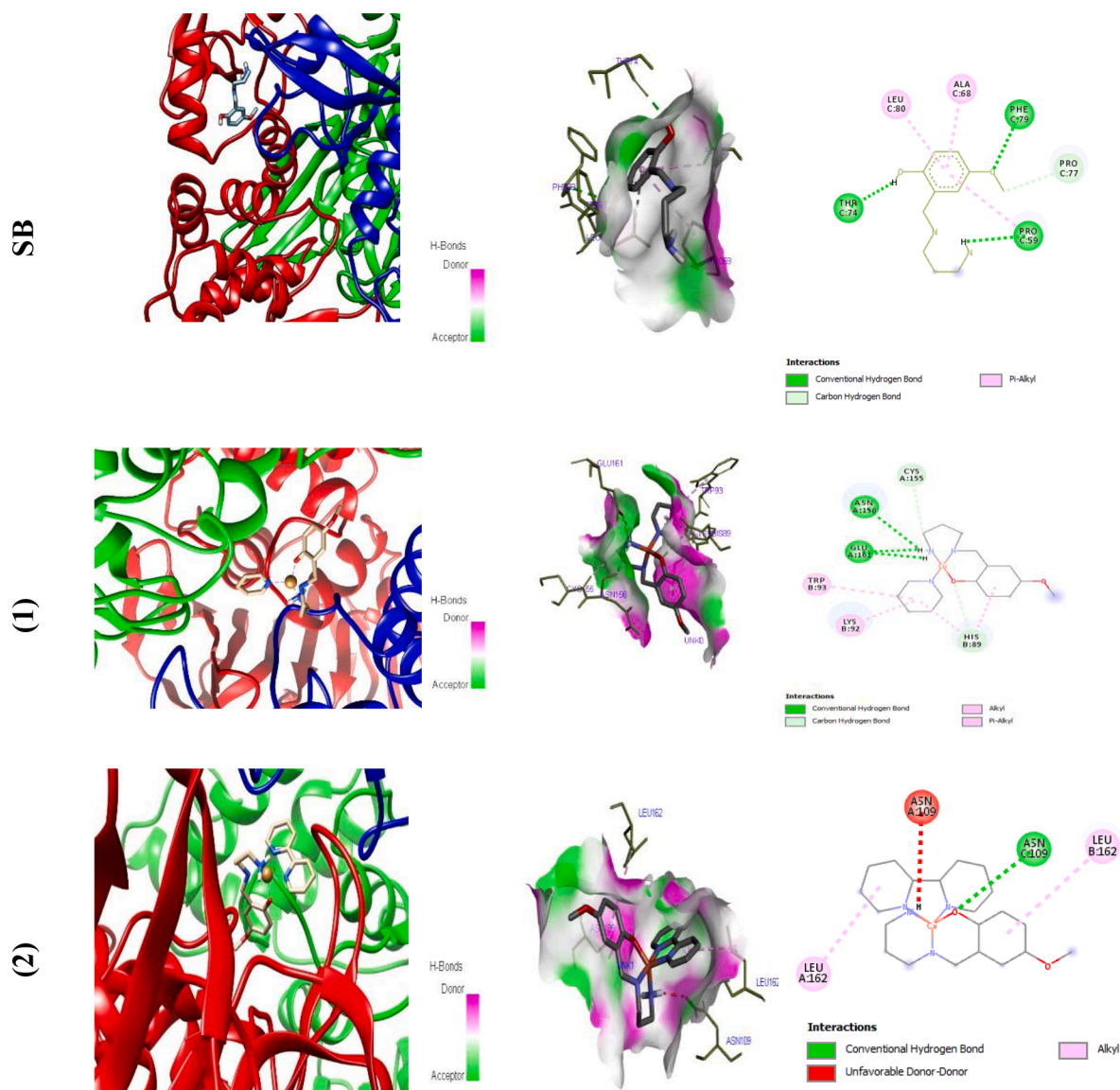


Fig. 6. The molecular docking results of (SB), (1), (2), (3) and Favipiravir with 6W9C. (a) Molecular docking (b) H. bond Receptor-side surface interactions and (c) 2D-diagram representations.

6WQF were also H of NH_2 ligand (HBD), OH of Aldehyde (HBD) N of ligand (HBA), OH of Aldehyde (HBA) and O of OCH_3 which were able to make H. bond interactions; and C of the ligand as (HYD) participates in interactions. The functional groups for (1) interacting with 6LU7 are N of NH_2 from SB ligand (HBD) which was able to make H. bond interactions, O of aldehyde and N of pyridine (HBA) which were able to make C—H. bond interactions, and pyridine ring (HYD) which was able to make Alkyl Hyd. Interactions. Functional groups for (1) to 6W9C were N of NH_2 from SB ligand (HBD) which was able to make H. bond interaction, N of pyridine, O of OCH_3 group and O of aldehyde (HBA) which were able to make C—H. bond interactions, and the ring of pyridine (HYD) which was able to make Alkyl Hyd. Interaction.

Functional groups for (1) to 6WQF were also N of NH_2 ligand (HBD) which was able to make H. bond interaction, N of pyridine and O of aldehyde (HBA) which were again able to make C—H. bond interactions, and a ring of pyridine (HYD) which was able to make Alkyl Hyd.

Interaction. Functional groups for (2) to 6LU7 were also, to some extent, similar to (1). N of NH_2 from SB ligand (HBD) could make H. bond interactions, O of OCH_3 and N of bpy (HBA), and the ring of bpy and ring of aldehyde (HYD) could make Alkyl Hyd. and π -Alkyl Hyd. Interactions. The aldehyde aromatic ring was also able to make Alkyl Hyd. and π -Alkyl Hyd. interactions. Functional groups for (2) to 6W9C were O of aldehyde (HBA, H. bond interaction). Functional groups for (2) to 6WQF were ring of bpy (HYD, Alkyl Hyd. and π -Alkyl Hyd.) and N of NH_2 from SB ligand (HBD, H. bond interaction). Functional groups for (3) to 6LU7 were N of NH_2 (HBD, H. bond interaction), O of OCH_3 (HYD). Functional groups for (3) to 6W9C were N of NH_2 (HBD), O of aldehyde and N of NH_2 (HBA) which were able to make H. bond interactions. Functional groups for (3) to 6WQF were phen ring (Alkyl Hyd. and π -Alkyl Hyd. Interactions) and O of OCH_3 group (HYD), CH_3 of OCH_3 group (HBA, C—H. bond interactions), N of NH_2 (HBD, C—H. bond interactions) and phen ring (Alkyl Hyd. and π -Alkyl Hyd.

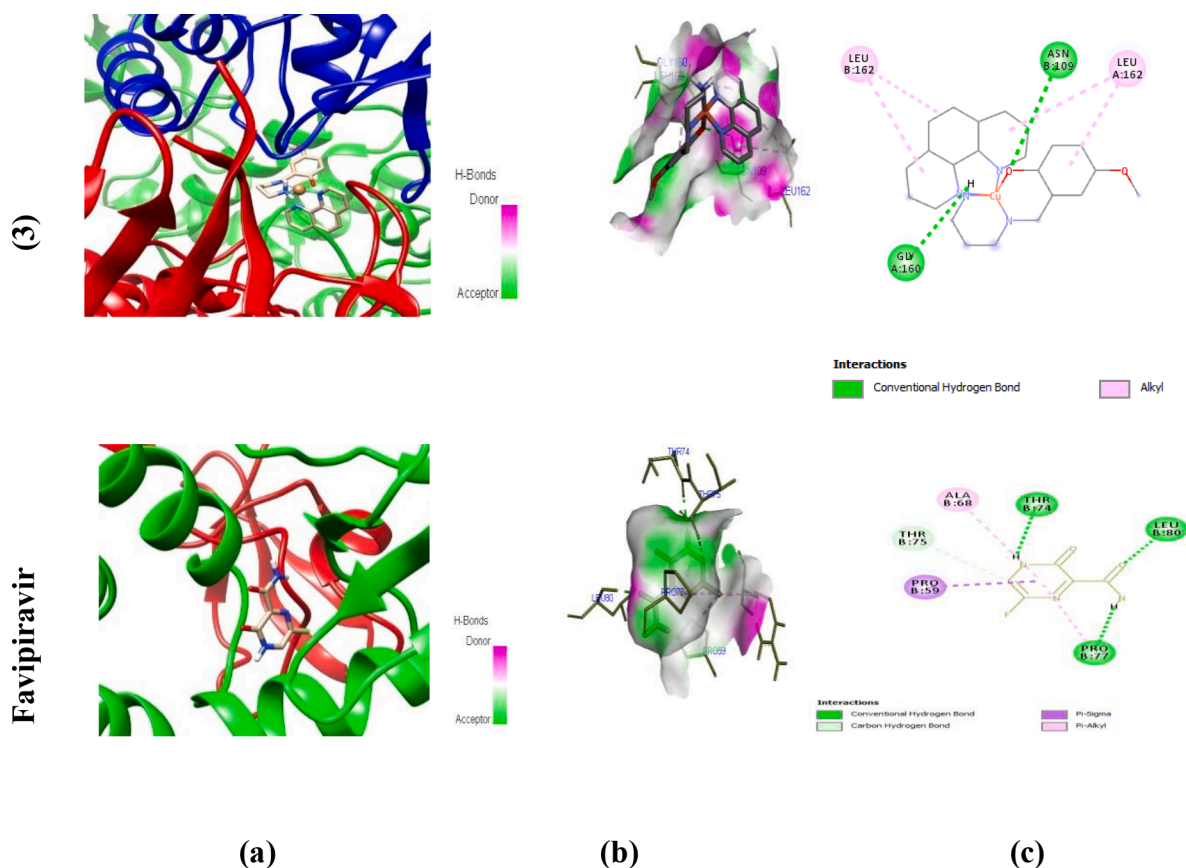


Fig. 6. (continued).

Table 6

Docking results of the complexes (1), (2), (3) and Favipiravir to 6WQF (kcal. mol⁻¹).

	SB	(1)	(2)	(3)	Favipiravir
Estimated free energy of binding ^a	-5.97	-7.66	-7.46	-7.75	-4.19
Final intermolecular energy	-8.06	-8.26	-7.75	-8.04	-4.48
vdW + H-bond + desolve Energy	-6.93	-7.7	-6.20	-6.98	-4.42
Electrostatic energy	-1.13	-0.56	-1.55	-1.06	-0.27
Final total internal energy	-0.15	-0.36	-0.04	-0.04	-0.42
Torsional free energy	2.09	0.6	0.3	0.3	0.3
Unbound system's energy	-0.15	-0.36	-0.04	-0.04	-0.42

$$^a \Delta G_{\text{binding}} = \Delta G_{\text{vdW}} + \text{hb} + \text{desolve} + \Delta G_{\text{elec}} + \Delta G_{\text{Total}} + \Delta G_{\text{Tor}} - \Delta G_{\text{Unb}}$$

interactions). One must keep in mind that interactions at shorter distances are more important. The pharmacophore results correspond to the docking results in tables S.1-3. To show the merit of the work, a comparison of the binding energies of other similar complexes to 6LU7 is shown in Table 8. As could be seen from Table 8, our results are similar and in some cases better than previously reported ones.

4. Conclusion

Three new mixed-ligand complexes with an unsymmetrical Schiff base ligand and *N*-donor heterocyclic coligands were synthesized and characterized. Crystal structures of two of the complexes were obtained by SCXRD. Molecular docking and pharmacophore modelings were performed to investigate the interactions between these three complexes as well as the main Schiff base ligand with three main proteases of SARS-

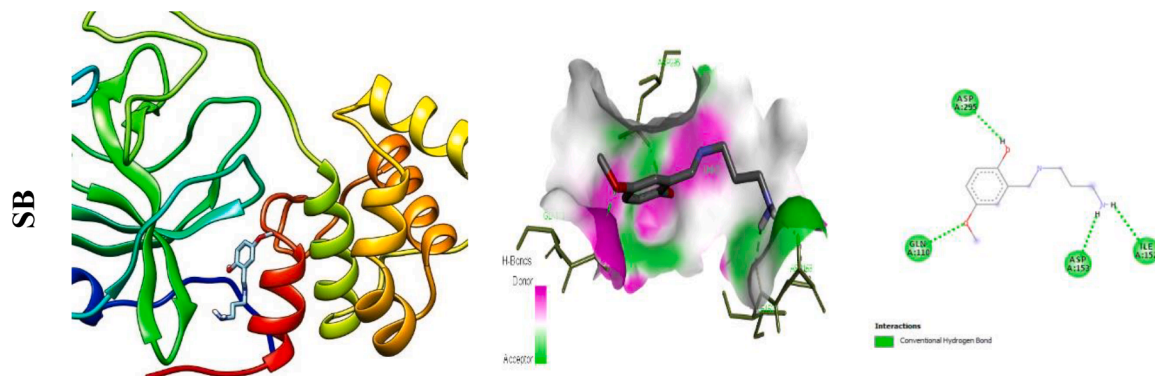


Fig. 7. The molecular docking results of (SB), (1), (2), (3) and Favipiravir with 6WQF. (a) Molecular docking (b) H. bond Receptor-side surface interactions and (c) 2D-diagram representations.

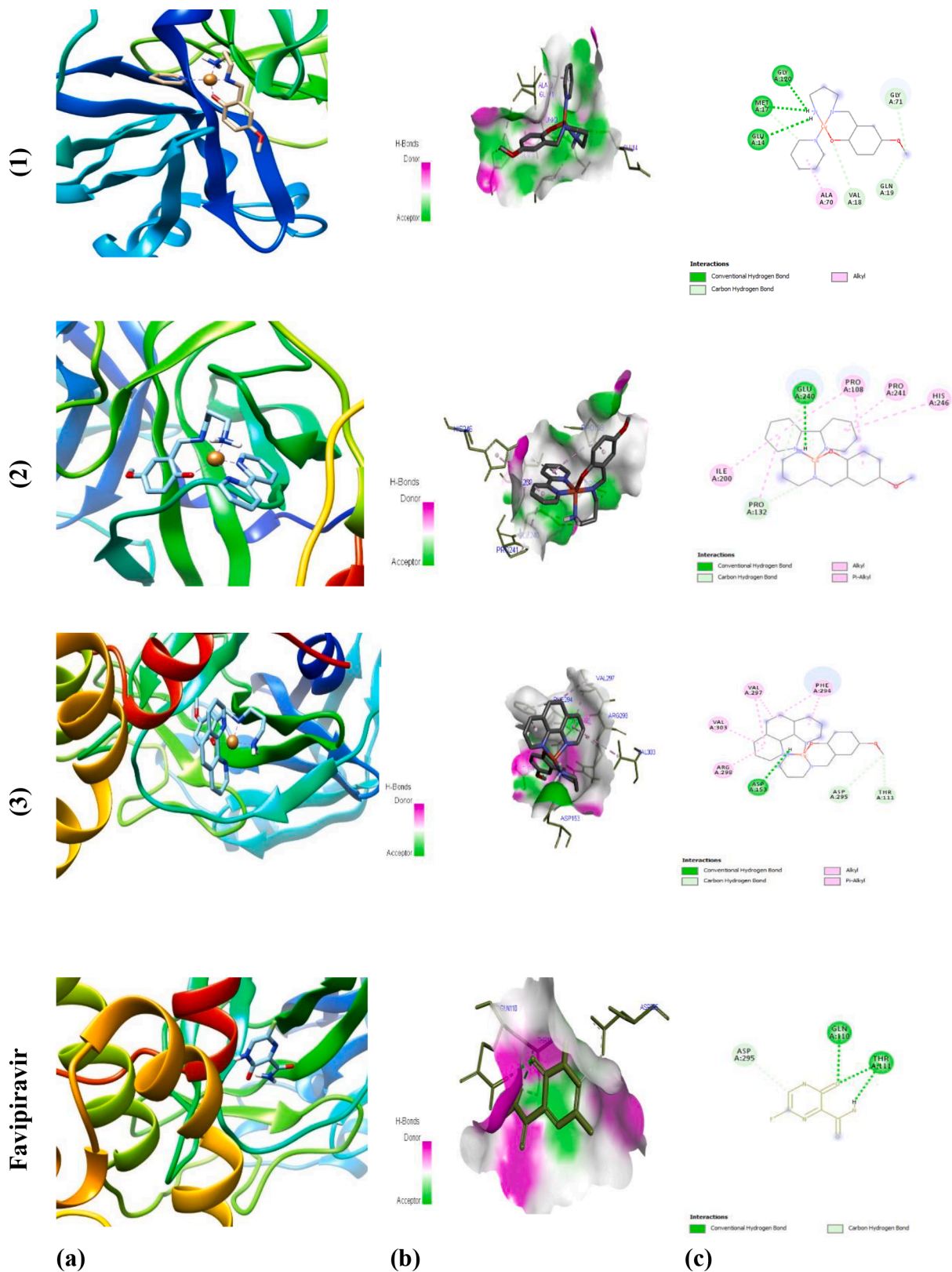


Fig. 7. (continued).

CoV-2. The following results were obtained from molecular docking and pharmacophore studies:

1. Complex (3) showed better docking scores with the studied proteases. The order of the binding best energies for (3) were as follows

6LU7 > 6WQF > 6W9C. All of the complexes showed better results than Favipiravir. Besides, the order of the scores were (3)>(2)>(1)>(SB) which could be attributed to the presence of more aromatic rings. The higher the number of the aromatic rings, the higher the

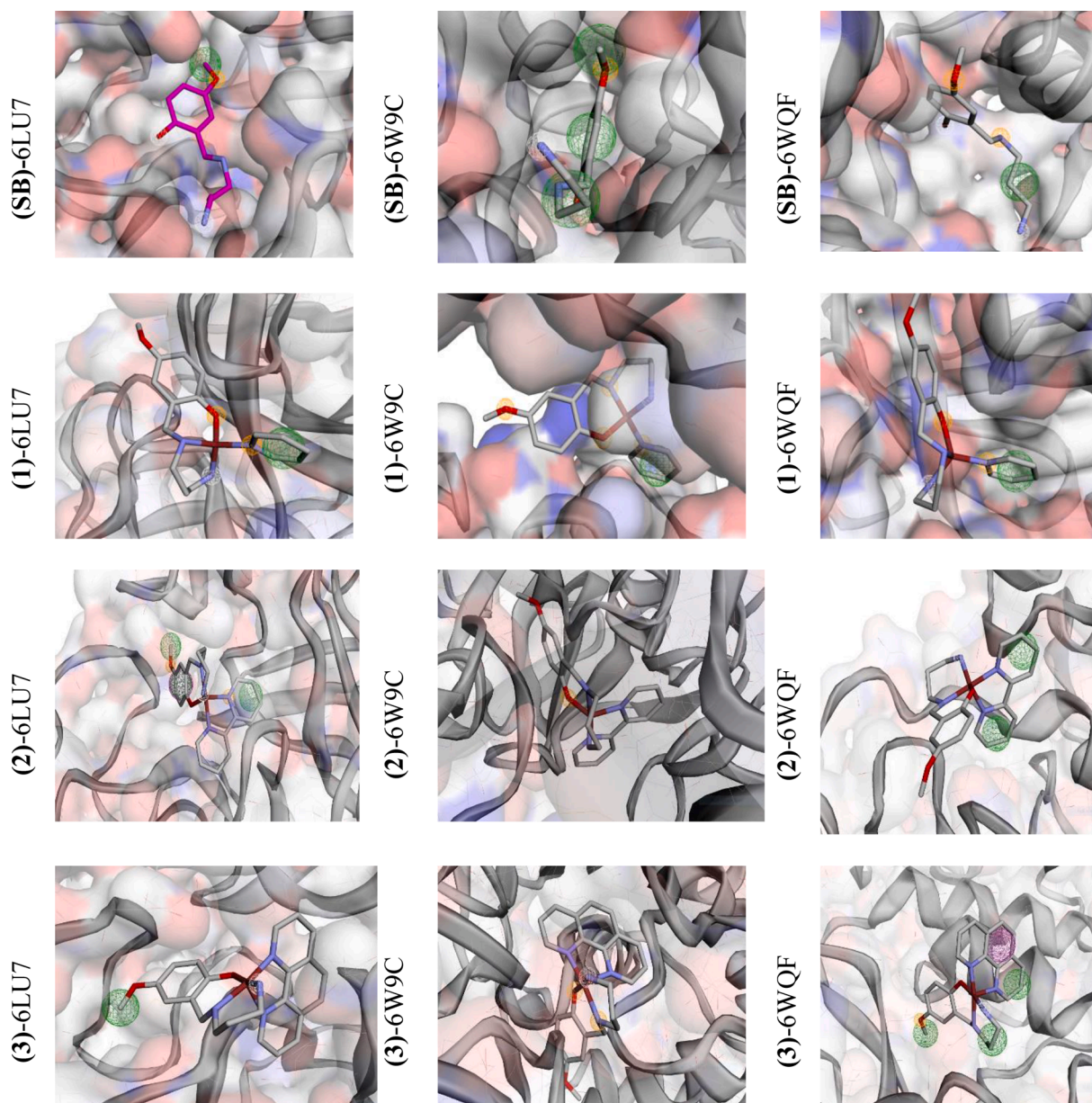


Fig. 8. Pharmacophore model study of the ligand (SB), and complexes (1), (2) and (3) to 6LU7, 6W9C and 6WQF.

Table 7
Uniquely identified pharmacophoric features of compounds.

Complex	PDB code	HBD*	HBA*	HYD*	Aromatic ring*
(SB)	6LU7	2	2	1	-
	6W9C	2	2	3	-
	6WQF	2	4	1	-
(1)	6LU7	1	2	1	-
	6W9C	1	4	1	-
	6WQF	1	2	1	-
(2)	6LU7	1	2	3	1
	6W9C	-	1	-	-
	6WQF	1	-	2	-
(3)	6LU7	1	-	1	-
	6W9C	1	2	-	-
	6WQF	1	1	3	1

HBD: Hydrogen Bond Donor; HBA: Hydrogen Bond Acceptor, HYD: Hydrophobic.

affinity of these compounds to interact with the aminoacids at the active sites.

- The (SB) main ligand had greater effect on the drug/receptor interactions than the co-ligands. This could be rationalized based on the fact that the interactions of the (SB) moiety were observed at lower distances.
- The pharmacophore results confirmed the docking results.
- Our studies suggest that such complexes may merit further studies in the context of possible therapeutic agents for COVID-19.

Declaration of Competing Interest

The authors declare that they have no known competing financial interests or personal relationships that could have appeared to influence the work reported in this paper.

Table 8

Comparison of the binding energies of new and previously reported complexes obtained from molecular docking to 6LU7 (kcal.mol⁻¹).

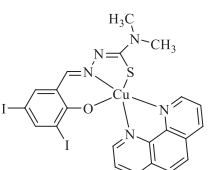
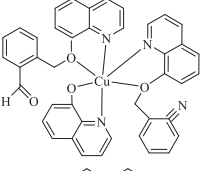
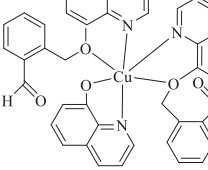
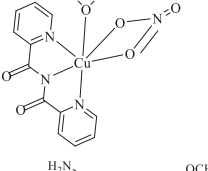
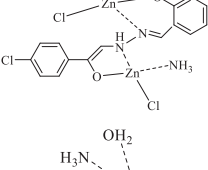
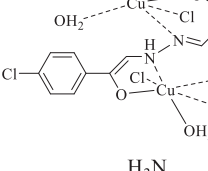
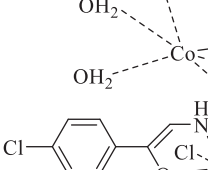
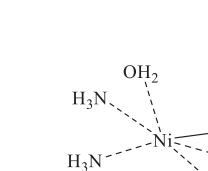
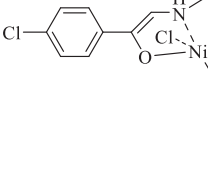
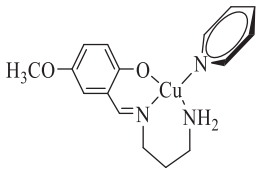
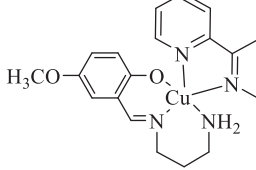
Complex	Binding energy	Reference
	-6.18	[19]
	-7.13	[20]
	-8.13	[20]
	-20.2	[29]
	-7.13	[30]
	-8.13	[30]
	-6.19	[30]
	-7.12	[30]
	-6.95	This work

Table 8 (continued)

Complex	Binding energy	Reference
	-7.31	This work
	-8.05	This work

Appendix A. Supplementary data

Supplementary data to this article can be found online at <https://doi.org/10.1016/j.poly.2022.115825>.

References

- [1] M. Pervaiz, S. Sadiq, A. Sadiq, U. Younas, A. Ashraf, Z. Saeed, M. Zuber, A. Adnan, Azo-Schiff base derivatives of transition metal complexes as antimicrobial agents, *Coord. Chem. Rev.* 447 (2021), 214128, <https://doi.org/10.1016/j.ccr.2021.214128>.
- [2] C. Verma, M.A. Quraishi, Recent progresses in Schiff bases as aqueous phase corrosion inhibitors: Design and applications, *Coord. Chem. Rev.* 446 (2021), 214105, <https://doi.org/10.1016/j.ccr.2021.214105>.
- [3] M. Liu, H. Yang, D. Li, Q. Yao, H. Wang, Z. Zhang, J. Dou, Zn and Cu complexes of o-van-gly Schiff base: Syntheses, crystal structures, fluorescence sensing and anticancer properties, *Inorg. Chim. Acta.* 522 (2021) 120384. doi:10.1016/j.ica.2021.120384.
- [4] R.V. Sakthivel, P. Sankudevana, P. Vennila, G. Venkatesh, S. Kaya, G. Serdaroglu, Experimental and theoretical analysis of molecular structure, vibrational spectra and biological properties of the new Co(II), Ni(II) and Cu(II) Schiff base metal complexes, *J. Mol. Struct.* 1233 (2021), 130097, <https://doi.org/10.1016/j.molstruc.2021.130097>.
- [5] M. Pellei, F. Del Bello, M. Porchia, C. Santini, Zinc coordination compounds as anticancer agents, *Coord. Chem. Rev.* 445 (2021), 214088, <https://doi.org/10.1016/j.ccr.2021.214088>.
- [6] S. Mahato, N. Meheta, M. Kotakonda, M. Joshi, M. Shit, A.R. Choudhury, B. Biswas, Synthesis, structure, polyphenol oxidase mimicking and bactericidal activity of a zinc-schiff base complex, *Polyhedron* 194 (2021), 114933, <https://doi.org/10.1016/j.poly.2020.114933>.
- [7] M. Diana, Symmetrical and un symmetrical salen-type Schiff base ligands and their transition metal complexes, PhD thesis, (2003) ProQuest Number: U642409.
- [8] L. Rigomonti, A. Forni, R. Pievo, J. Reedijk, A. Pasini, Copper(II) compounds with NNO tridentate Schiff base ligands: effect of subtle variations in ligands on complex formation, structures and magnetic properties, *Inorg. Chim. Acta.* 387 (2012) 373–382, <https://doi.org/10.1016/j.ica.2012.02.030>.
- [9] I.A. Guedes, L.S.C. Costa, K.B. dos Santos, A.L.M. Karl, G.K. Rocha, I.M. Teixeira, M.M. Galheigo, V. Medeiros, E. Krempser, F.L. Custódio, H.J.C. Barbosa, M. F. Nicolás, L.E. Dardenne, Drug design and repurposing with DockThor-VS web server focusing on SARS-CoV-2 therapeutic targets and their non-synonym variants, *Sci. Rep.* 11 (1) (2021), <https://doi.org/10.1038/s41598-021-84700-0>.
- [10] X.-Y. Meng, H.-X. Zhang, M. Mezei, M. Cui, Molecular docking: a powerful approach for structure-based drug discovery, *Curr. Comput. Aid. Drug.* 7 (2011) 146–157, <https://doi.org/10.2174/157340911795677602>.
- [11] L.G. Ferreira, R.N. Dos Santos, G. Oliva, A.D. Andricopulo, Molecular docking and structure-based drug design strategies, *Molecules.* 20 (2015) 13384–13421, <https://doi.org/10.3390/molecules200713384>.
- [12] M. Stekláč, D. Zajaček, L. Bučinský, 3CLpro and PLpro affinity, a docking study to fight COVID19 based on 900 compounds from PubChem and literature. Are there new drugs to be found? *J. Mol. Struct.* 1245 (2021) 130968.
- [13] S.A. Almalki, T.M. Bawazeer, B. Asghar, A. Alharbi, M.M. Aljohani, M.E. Khalifa, N. El-Metwaly, Synthesis and characterization of new thiazole-based Co(II) and Cu

- (II) complexes; therapeutic function of thiazole towards COVID-19 in comparing to current antivirals in treatment protocol, *J. Mol. Struct.* 1244 (2021), 130961, <https://doi.org/10.1016/j.molstruc.2021.130961>.
- [14] A. Chhetri, S. Chhetri, P. Rai, D.K. Mishra, B. Sinha, D. Brahman, Synthesis, characterization and computational study on potential inhibitory action of novel azo imidazole derivatives against COVID-19 main protease (Mpro: 6LU7), *J. Mol. Struct.* 1225 (2021), 129230, <https://doi.org/10.1016/j.molstruc.2020.129230>.
- [15] H.Y. Odabasoglu, T. Erdogan, F. Karci, Synthesis & characterization of heterocyclic disazo-azomethine dyes and investigating their molecular docking & dynamics properties on acetylcholine esterase (AChE), heat shock protein (HSP90 α), nicotinamide N-methyl transferase (NNMT) and SARS-CoV-2 (2019-nCoV, COVID-19) main protease (Mpro), *J. Mol. Struct.* 1252 (2022), 131974, <https://doi.org/10.1016/j.molstruc.2021.131974>.
- [16] Z. Qiao, N. Wei, L. Jin, H. Zhang, J. Luo, Y. Zhang, K. Wang, The Mpro structure-based modifications of ebiselen derivatives for improved antiviral activity against SARS-CoV-2 virus, *Bioorg. Chem.* 117 (2021), 105455, <https://doi.org/10.1016/j.bioorg.2021.105455>.
- [17] G.M. Sheldrick, SHELXS-97 and SHELXL-97, Program for Crystal Structure Solution and Refinement, University of Gottingen, Gottingen, 1997.
- [18] G.M. Sheldrick, Crystal structure refinement with SHELXL, *Struct. Chem.* 71 (2015) 3–8, <https://doi.org/10.1107/S2053229614024218>.
- [19] B. Mohan, M. Choudhary, Synthesis, crystal structure, computational study and anti-virus effect of mixed ligand copper (II) complex with ONS donor Schiff base and 1,10-phenanthroline, *J. Mol. Struct.* 1246 (2021), 131246, <https://doi.org/10.1016/j.molstruc.2021.131246>.
- [20] A. Ali, N. Sepay, M. Afzal, N. Sepay, A. Alarifi, M. Shahid, M. Ahmad, Molecular designing, crystal structure determination and in silico screening of copper (II) complexes bearing 8-hydroxyquinoline derivatives as anti-COVID-19, *Bioorg. Chem.* 110 (2021), 104772, <https://doi.org/10.1016/j.bioorg.2021.104772>.
- [21] M.U. Mirza, S. Ahmad, I. Abdullah, M. Froeyen, Identification of novel human USP2 inhibitor and its putative role in treatment of COVID-19 by inhibiting SARS-CoV-2 papain-like (PLpro) protease, *Comput. Biol. Chem.* 89 (2020), 107376, <https://doi.org/10.1016/j.compbiolchem.2020.107376>.
- [22] S.A. Almalki, T.M. Bawazeer, B. Asghar, A. Alharbi, M.M. Aljohani, M.E. Khalifa, N. El-Metwaly, Synthesis and characterization of new thiazole-based Co (II) and Cu (II) complexes; therapeutic function of thiazole towards COVID-19 in comparing to current antivirals in treatment protocol, *J. Mol. Struct.* 1244 (2021), 130961, <https://doi.org/10.1016/j.molstruc.2021.130961>.
- [23] Z. Albobaleidi, M.H. Esfahani, M. Behzad, A. Abbasi, Mixed ligand Cu (II) complexes of an unsymmetrical Schiff base ligand and N-donor heterocyclic co-ligands: investigation of the effect of co-ligand on the antibacterial properties, *Inorg. Chim. Acta.* 499 (2020), 119185, <https://doi.org/10.1016/j.ica.2019.119185>.
- [24] S. Alimirzaei, M. Behzad, S. Abolmaali, Z. Abbasi, Mixed-ligand copper complexes with unsymmetrical tridentate Schiff base ligands and 2,2'-bipyridine: synthesis, x-ray crystallography and antibacterial properties, *J. Mol. Struct.* 1200 (2020), 127148, <https://doi.org/10.1016/j.jca.2019.119185>.
- [25] M. Hasanzadeh Esfahani, M. Behzad, Crystal structure and antibacterial properties of a new dinuclear copper complex based on an unsymmetrical NN'O type Schiff base ligand, *J. Coord. Chem.* 73 (2020) 154–163, <https://doi.org/10.1080/00958972.2020.1725492>.
- [26] M. Hasanzadeh Esfahani, H. Iranmanesh, J.E. Beves, M. Kaur, J.P. Jasinski, M. Behzad, Crystal structures and antibacterial properties of Cu (II) complexes containing an unsymmetrical N2O Schiff base ligand and bidentate N-donor heterocyclic co-ligands, *J. Coord. Chem.* 72 (2019) 2326–2336, <https://doi.org/10.1080/00958972.2019.1643846>.
- [27] M.S.S. Adam, S. Shaaban, M.E. Khalifa, M. Alhasani, N. El-Metwaly, New Cu (II) and VO (II)-O, N, O-arylhyazone complexes: biological evaluation, catalytic performance, ctDNA interaction, DFT, pharmacophore, and docking simulation, *J. Mol. Liq.* 335 (2021), 116554, <https://doi.org/10.1016/j.molliq.2021.116554>.
- [28] A.M. Abu-Dief, N.M. El-Metwaly, S.O. Alzahrani, F. Alkhatib, M.M. Abualnaja, T. El-Dabea, M.A. El-Aleem, A.A. El-Ry, Synthesis and characterization of Fe(III), Pd(II) and Cu(II)-thiazole complexes; DFT, pharmacophore modeling, in-vitro assay and DNA binding studies, *J. Mol. Liq.* 326 (2021), 115277, <https://doi.org/10.1016/j.molliq.2021.115277>.
- [29] L.H. Abdel-Rahman, M.T. Basha, B.S. Al-Farhan, M.R. Shehata, S.K. Mohamed, Y. Ramlil, [Cu (dipicolinoylamide)(NO₃)(H₂O)] as anti-COVID-19 and antibacterial drug candidate: design, synthesis, crystal structure, DFT and molecular docking, *J. Mol. Struct.* 1247 (2022), 131348, <https://doi.org/10.1016/j.molstruc.2021.131348>.
- [30] M.S. Refat, A. Gaber, W.F. Alsanie, M.I. Kobeasy, R. Zakaria, K. Alam, Utilization and simulation of innovative new binuclear Co (ii), Ni (ii), Cu (ii), and Zn (ii) diimine Schiff base complexes in sterilization and coronavirus resistance (Covid-19), *Open. Chem.* 19 (2021) 772–784, <https://doi.org/10.1515/chem-2021-0068>.